Image Thresholding by Variational Minimax Optimization

Baidya Nath Saha and Nilanjan Ray
University of Alberta
Edmonton, Alberta, Canada
{baidya, nray1} @cs.ualberta.ca

Abstract

In this paper we introduce an adaptive image thresholding technique via minimax optimization of a novel energy functional that consists of a non linear convex combination of an edge sensitive data fidelity term and a regularization term. While the proposed data fidelity term compels the threshold surface to intersect the image surface only at high gradient places, the regularization term enforces smoothness in the threshold surface. To the best of our knowledge, all the previously proposed energy functional-based adaptive image thresholding algorithms rely on manually setting the weighting parameters to achieve a balance between the data fidelity and the regularization terms. In contrast, we use minimax principle to automatically find this weighting parameter value, as well as the spatially adaptive threshold surface. Our conscious choice of the energy functional permits a variational formulation within the minimax principle leading to a globally optimum solution. The proposed variational minimax optimization is carried out with an iterative gradient descent line search technique, which we experimentally demonstrate to be computationally far more efficient than the Fibonacci search applied to find the minimax solution. Our method shows promising results to find lung boundary from magnetic resonance imagery– up to 28% improvement on segmentation score (Pratt's Figure of Merit) over other competing methods. Visual demonstrations of the application of the proposed method on different benchmark images reveal that that our method preserves better texture/edge information than other competing methods.

Keywords: minimax principle, variational calculus, image thresholding.

1. Introduction

Image thresholding is an image pixel labeling problem. It aims to classify pixels of an image into two classes: foreground and background. Typically, a pixel is classified as foreground if the image intensity at the pixel exceeds a threshold value; otherwise it is classified as a background pixel. Thresholding is a well known pre-processing step for image segmentation. It is widely used in automatic target recognition, industrial applications of computer visions and medical/biomedical image analysis.

In general there are two types of image thresholding techniques available: global and local. In the global thresholding technique a gray level image is converted into a binary image based on an image intensity value called global threshold which is fixed in the whole image domain whereas in local thresholding technique, threshold value can vary from one pixel location to next. Thus, global thresholding converts an input image I to a binary image G as follows: $G(i, j) = 1$ for $I(i, j) \geq T$, or, $G(i, j) = 0$ for $I(i, j) < T$, where T is the threshold, $G(i, j) = 1$ for foreground and $G(i, j) = 0$ for background. Whereas, for a local threshold, the threshold T is a function over the image domain, *i.e.*, $T = T(x, y)$. In addition, if in constructing the threshold value/surface the algorithm adapts itself to the image intensity values, then it is called dynamic or adaptive threshold.

In a general setting, thresholding can be expressed as a test operation that tests against a function T of the form [7]: $T = T[x, y, h, I]$, where, I is the input image and h denotes some local property of this point– for example, the average gray level of a neighbourhood centered on (x, y).

Threshold selection depends on the information available in the gray level histogram of the image. We know that an image function $I(x, y)$ can be expressed as the product of a reflectance function and an illumination function based on a simple image formation model. If the illumination component of the image is uniform then the gray level

histogram of the image is clearly bimodal, because the gray levels of object pixels are significantly different from the gray levels of the background. It indicates that one mode is populated from object pixels and the other mode is populated from background pixels. Then objects could be easily partitioned by placing a single global threshold at the neck or valley at the histogram. However, in reality bimodality in histograms does not occur very often. Consequently, a fixed threshold level based on the information of the gray level histogram will fail totally to separate objects from the background. In this scenario we turn our attention to adaptive local threshold surface where threshold value changes over the image domain to fit the spatially changing background and lighting conditions.

Over the years many threshold selection methods have been proposed. Otsu has suggested a global image thresholding technique where the optimal global threshold value is ascertained by maximizing the between-class variance with an exhaustive search [14]. Sahoo *et al.* [17] claim that Otsu's method is suitable for real world applications with regard to uniformity and shape measures. Though Otsu's method is one of the most popular methods for global thresholding, it does not work well for many real world images where a significant overlap exists in the gray level histogram between the pixel intensity values of the objects and the background due to un-even and poor illumination.

Kittler and Illingworth [8] characterize the image by a Gaussian mixture of foreground and background pixels and address a minimum error Gaussian-density fitting problem. They use either an exhaustive or an iterative search to optimize the average pixel classification error rate.

On the other hand, local thresholding method is superior to the global ones for poor and unevenly illuminated images. Niblack proposes a local thresholding technique based on the local mean and local standard deviation [13]. The drawback of this algorithm is to determine the size of the neighborhood that is set by the user and it depends on the

information available in the images. The window size should be small enough to preserve the local details and at the same time, it should be large enough to suppress noise.

For unevenly illuminated images one can fit a plane or biquadratic function to match the background gray-level variations [9]. A more advanced method tries to generate a threshold surface where the threshold level changes dynamically over the image pixel to pixel [3]. Milgram *et al.* use gradient or edge information to segment images and assumed that different objects may have different thresholds, but each object has a fixed threshold with respect to its background [12].

Yanowitz and Bruckstein [22] have incorporated the concepts of threshold surface and suggested an algorithm where the threshold surface is determined by the interpolation of the intensity values at high magnitudes of image intensity gradient. The computational complexity of the successive over-relaxation method used in Yanowitz and Bruckstein's algorithm is prohibitively expensive: O (N^3) for an $N \times N$ image. Moreover, the technique uses a mean filter in the processing stage to eliminate the noise that reduces the contrast of the image and consequently affects the segmentation results. Also, there is no good algorithm to choose the value for the gradient magnitude threshold. Choosing improper threshold value leads to false object boundary points affecting the following steps of the algorithm and producing poor results.

Yan *et al.* [21] propose a multistage adaptive thresholding where they consider two global thresholds: pixels having gray values lower than the low threshold value are considered as the background, pixels with intensity greater than the high threshold value are considered as objects and the pixels with gray values in between the two threshold values are considered based on local image statistics of mean and variance within a variable neighborhood. The values of two global thresholds are determined using Otsu's

multilevel threshold with exhaustive search technique or percentile statistics. The window size of the neighborhood is determined by add-hoc trial and error method.

Chan *et al.* [2] propose a variational formulation of adaptive thresholding technique based on the principle advocated by Yanowitz and Bruckstein [22]. Whereas Yanowitz and Bruckstein's method involves pre and post processing steps followed by solving a Laplace's equation, Chan and *et al.* [2] reduce their solution to solving a Poisson equation with only one user supplied scalar parameter.

The interpolation in Yanowitz and Bruckstein's algorithm does not consider the relationship between the threshold surface and the image surface which causes either black stains on white background or vice versa. Liu *et al*. [11] propose an active surface–based adaptive thresholding algorithm by a repulsive external force. In this model, a Gaussian external repulsive force is designed to keep the active surface away from the image surface while the smoothness constraint and the boundary condition on the threshold surface restrain it from moving far away. Shen and Ip [19] use a Hopfield neural network for an active surface paradigm like Liu *et al.* [11]. Li *et al.* compares different thresholding algorithms for segmenting aurora oval boundary from spacecraft UV imagery and they showed that local adaptive thresholding algorithm showed better results than other thresholding techniques [10]. Sezgin and Sankur have made a recent survey on image thresholding [18].

To the best of our knowledge, all the available local thresholding techniques, including the ones using energy functional minimization, have manually tuned parameters that need to be adjusted for differently illuminated images by trial and error method. The values of these parameters vary significantly for different images. To mitigate the effort of tuning parameters, in this paper, we introduce an adaptive local image thresholding method based on energy functional minimization, where the

weighting parameters for the data and the regularization terms do not need to be supplied by a user. The proposed energy functional consists of a non-linear convex combination of a data term and a regularization term. The data term encourages the threshold surface to intersect the image surface at high gradient location and the regularization term imposes smoothness on the threshold surface. In order to find out the solution, *i.e.*, the desired threshold surface, we propose a variational minimax (VM) optimization. The VM algorithm consists of two interleaved iterative steps: maximization with respect to the weighting parameter and variational minimization with respect to the threshold surface. We demonstrate that our conscious choice of the energy functional creates a unique saddle point and the VM algorithm finds this saddle point containing the desired solution. We guarantee this unique saddle point by making the energy functional strictly concave with respect to the weighting parameter and strictly convex with respect to the threshold surface.

In this connection, it is worth mentioning that Gennert and Yuille have proposed a minimax solution for general non-convex energy functional by repeated Fibonacci search [6]. Their method consists of multiple minimization computations for different values of the weighting parameter dictated by a Fibonacci sequence. In contrast the proposed VM method avoids multiple minimization computations by virtue of a deliberate choice of concavo-convex energy functional. As a result, with respect to computations, we compare VM method favorably against the Fibonacci search technique (see Section 4.3 for comparisons).

The outline of this paper is as follows. In Section 2 our proposed threshold algorithm is described. In Section 3 numerical implementation is furnished in details. Experimental results are presented in Section 4. Section 5 contains directions for future work and conclusion.

2. Proposed Method

Let us assume that $I(x, y)$ and $T(x, y)$ respectively are the image and threshold functions. Our proposed energy functional is as follows:

$$E(T;\alpha) = \sqrt{1-\alpha^2}\,E_1(T) + \alpha E_2(T), \tag{1}$$

where,

$$E_1(T) = \frac{1}{2}\iint h(x,y)\big(I(x,y) - T(x,y)\big)^2\,dxdy, \tag{2}$$

$$E_2(T) = \frac{1}{2}\iint |\nabla T(x,y)|^2\,dxdy, \tag{3}$$

with $h(x, y)$ defined as:

$$h(x,y) = \frac{|\nabla I(x,y)|^q}{\max\left(|\nabla I(x,y)|^q\right)}. \tag{4}$$

Here $\alpha \in [0,1]$ is the weighting parameter. The first component of the energy functional dictates the threshold surface to intersect the image surface at high gradient places and the second component of the energy functional is responsible for smoothing the threshold surface.

The value of the exponent q in equation (4) is generally taken as 2 to describe the gradient strength of an image. However, sometimes it may be useful to find its value by simple cross-validation as described in Section 4. Note that the energy functional E in (1) is a concave function with respect to α and a convex functional with respect to T (proof in Appendix A and B).

To find the optimum threshold surface, we seek the minimax solution: $\max_{\alpha}\min_{T} E(T;\alpha)$. Minimax criterion minimizes the cost E in the worst possible case, and hence provides a very conservative solution. When the weights for the two components are unknown and/or hard to determine, minimax principle provides a way to find them

out. Because of the concavo-convex nature of E with respect to α and T, it is possible to interchange the order of the max and the min, because the duality gap is zero [16]:

$$T^* = \arg\max_{\alpha}\min_{T} E(T;\alpha) = \arg\min_{T}\max_{\alpha} E(T;\alpha). \quad (5)$$

We first differentiate E in (1) with respect to α and find the maximum value α^* by equating the derivative to zero:

$$\alpha^* = \frac{E_2(T)}{\sqrt{(E_1(T))^2 + (E_2(T))^2}}. \quad (6)$$

Next, we minimize E using gradient descent technique for T keeping this value α^* for α to be fixed (see Appendix C for a derivation):

$$\frac{\partial T}{\partial t}(x,y) = \sqrt{1-(\alpha^*)^2}\left(h(x,y)(I(x,y)-T(x,y))\right) + \alpha^*\left(\nabla^2 T(x,y)\right) \quad (7)$$

The algorithm Variational Minimax (VM) iteratively solves the minimax problem as follows.

Algorithm Variational Minimax

Initialize: $T \leftarrow I$

While convergence/maximum iterations not reached

Compute $E_1(T)$ and $E_2(T)$ via equation (2) and (3)

Compute: $\alpha^* \leftarrow \frac{E_2(T)}{\sqrt{(E_1(T))^2 + (E_2(T))^2}}$

Update T via equation (7)

End while

3. Numerical Implementation

Equation (7) is essentially a heat equation with a source term $\sqrt{1-(\alpha^*)^2}\,(h(x,y)(I(x,y))-T(x,y))$ [4]. A straightforward discrete implementation for (7) would be an explicit scheme as follows:

$$T_{i,j}^{t+1} = T_{i,j}^{t} + \tau\sqrt{1-(\alpha^*)^2}\,(h_{i,j}(I_{i,j} - T_{i,j}^{t})) + \tau\alpha^*(T_{i+1,j}^{t} + T_{i-1,j}^{t} + T_{i,j+1}^{t} + T_{i,j-1}^{t} - 4T_{i,j}^{t}), \quad (8)$$

where τ is the time step length of the iterative numerical scheme. In the explicit scheme, the finite difference analogs for $\nabla^2 T$ are written in given time level indexed by *t*. Convergence analysis shows that the step size τ should be less than or equal to ¼ [4] at each iteration. We have implemented steepest descent technique using line search algorithm to find the optimum value of step size τ at each iteration, instead of using a constant value for τ using the explicit scheme. The basic structure of the *k* th iteration is:

Step a: Determine a direction of search $\delta T_{i,j}^{(k)}$ where,

$$\delta T_{i,j}^{(k)} = \sqrt{1-(\alpha^{(k)})^2}\,(h_{i,j}(I_{i,j} - T_{i,j}^{(k)})) + \alpha^{(k)}(T_{i+1,j}^{(k)} + T_{i-1,j}^{(k)} + T_{i,j+1}^{(k)} + T_{i,j-1}^{(k)} - 4T_{i,j}^{(k)}).$$

Step b: Find $\tau^{(k)}$ by minimizing $E(T^{(k)} + \tau^{(k)}\delta T^{(k)})$ with respect to $\tau^{(k)}$.

Step c: Set $T^{(k+1)} = T^{(k)} + \tau^{(k)}\delta T^{(k)}$.

Since $E(T^{(k)} + \tau^{(k)}\delta T^{(k)}) = e_1 + \tau^{(k)} e_2 + (\tau^{(k)})^2 e_3$ (see Appendix D for details),

where, $e_1 = \frac{1}{2}\sum\left\{\alpha^{(k)}\|\nabla T\|^2 + \sqrt{1-(\alpha^{(k)})^2}\,h(I-T)^2\right\}$,

$$e_2 = \sum\left\{\alpha^{(k)}(\nabla T.\nabla(\delta T)) - \sqrt{1-(\alpha^{(k)})^2}\,h(I-T)(\delta T)\right\},$$

and $e_3 = \frac{1}{2}\sum\left\{\sqrt{1-(\alpha^{(k)})^2}\,h(\delta T)^2 + \alpha^{(k)}\|\nabla \delta T\|^2\right\}$.

The line search step, *i.e.*, **Step b** is fast: we increase $\tau^{(k)}$ starting from ¼, so long as the expression $e_1 + \tau^{(k)} e_2 + (\tau^{(k)})^2 e_3$ decreases. Note that e_1, e_2 and e_3 are independent of $\tau^{(k)}$.

4. Experimental Results

In this section we demonstrate that the proposed method can be used to find the boundaries of the lung cavity from Magnetic Resonance Image (MRI). We also demonstrate the capability of edge and texture preservation of the proposed method compared with other competing methods. Further, we compare the computations of the VM method with the conventional Fibonacci search technique.

4.1 Lung Boundary Extraction

We apply the VM algorithm on proton MRI slices to extract the lung boundaries shown in Fig. 1(a). Lung boundary extraction from proton MRI is of significance importance in clinical trials on some pulmonary diseases, because it helps to compute lung air intake volume that indicates the degree of progress of a pulmonary disease [15].

In this segmentation process we utilize VM as a pre-processing step. First, the value of edge indicator exponent q has been found experimentally from a small training set. Fig. 2 shows the values of q *vs.* Pratt's figure of merit (PFOM) [1] for three randomly chosen MRI slices. Initially the PFOM increases as the value of q increases and it stabilizes at q = 8 in Fig. 2. If the value of q is increased without bound, the edge indicator $h(x, y)$ will tend to zero for most pixel locations (x, y) and consequently the effect of edge sensitive data term on energy functional (1) decreases and the regularization term overpowers the data term. With the negligible data fidelity term the solution turns out to be that of an isotropic heat equation and will essentially be a global threshold value. Thus we limit the value of the exponent as 8. The results of VM method, Otsu and Fuzzy c-means algorithms are shown in Fig. 1(b), 1(c) and 1(d) respectively.

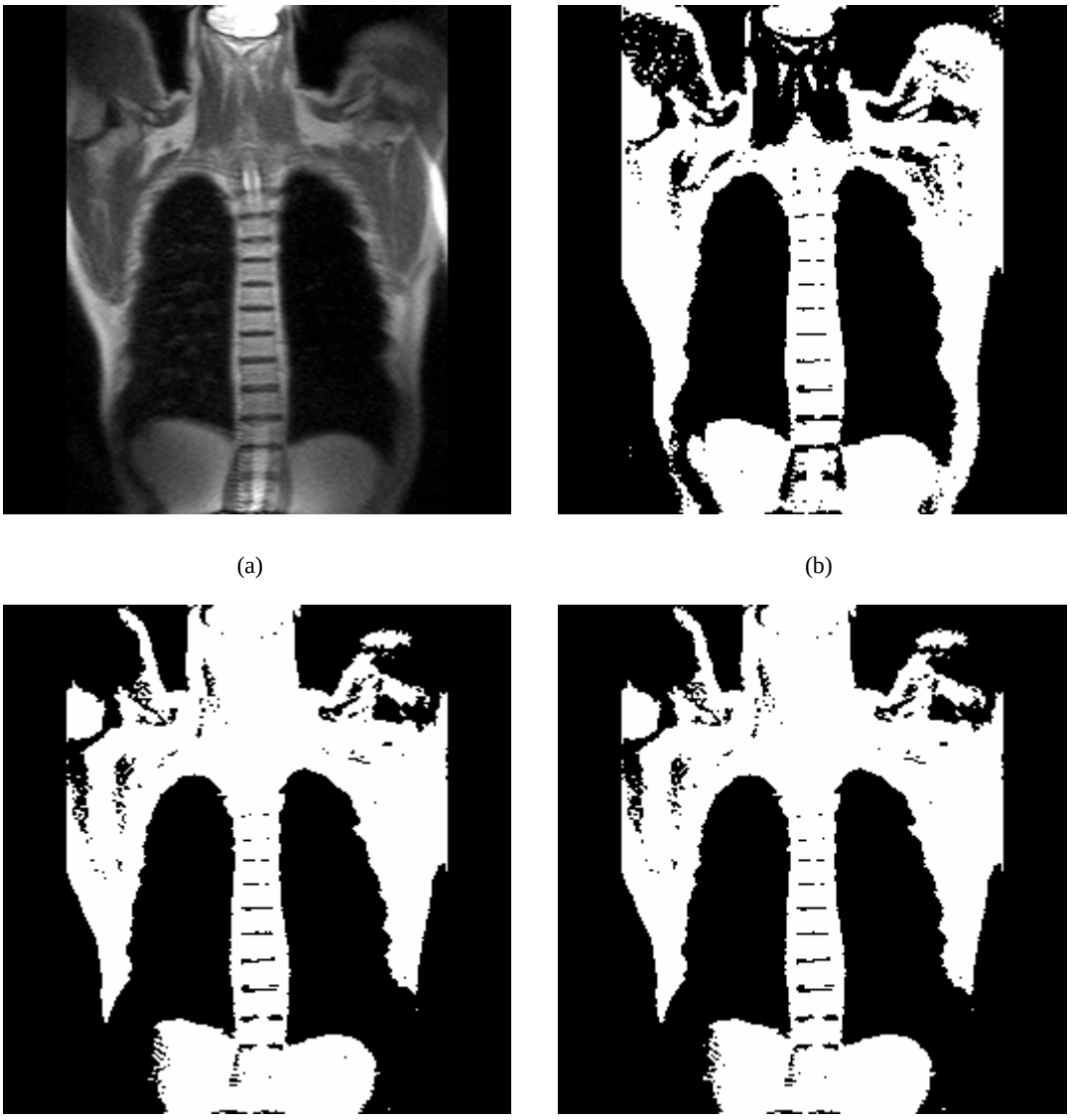

(a) (b)

(c) (d)

Fig. 1: (a) Proton MRI, (b) threshold by the proposed method, (c) threshold by Otsu's method [14], and (d) binarization by Fuzzy *c*-means classification.

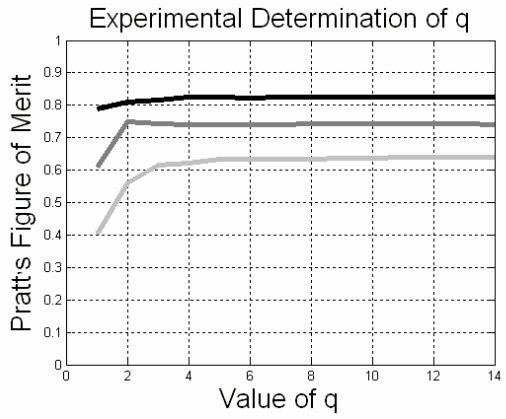

Fig. 2: PFOM for different values of q is shown. Three different lines represent PFOM for three different MRI slices.

Next, to complete the lung boundary extraction, the following morphological operations are performed on the binary image obtained by thresholding. Note that the two lung cavities are contained in the two black connected components located at the middle of the thresholded binary image shown in Fig. 1(b). These two black connected components are collected and their boundaries are found (shown in Fig. 3(a)). Now, we need to discard the unnecessary extended necks, if any, formed at the costophrenic angles, such as one shown here in Fig. 3(a) at the right cavity. Next, we compute the distance transform of the boundary image in Fig. 3(a) and threshold it at 5 to obtain the binary image shown in Fig. 3(b). Our empirical observations have led us to choose the threshold value of 5 here, as the neck width of extraneous portions hardly exceeds 10 pixels, *i.e.*, twice the chosen threshold value 5. Finally we perform watershed segmentation on the original proton image of Fig. 1(a) from two markers provided by the two white connected components from Fig. 3(b). The watershed boundaries are taken as the lung boundaries (shown in Fig. 3(c)).

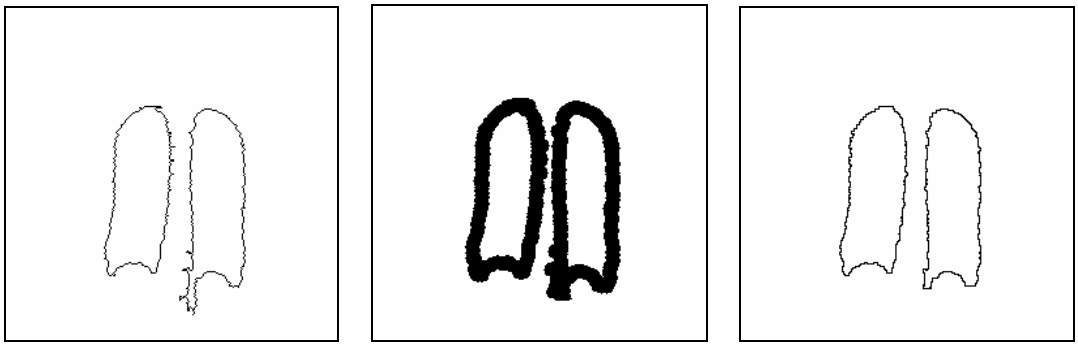

(a) (b) (c)

Fig. 3: Images of different steps of post processing operation required to find lung cavity from the thresholded binary image.

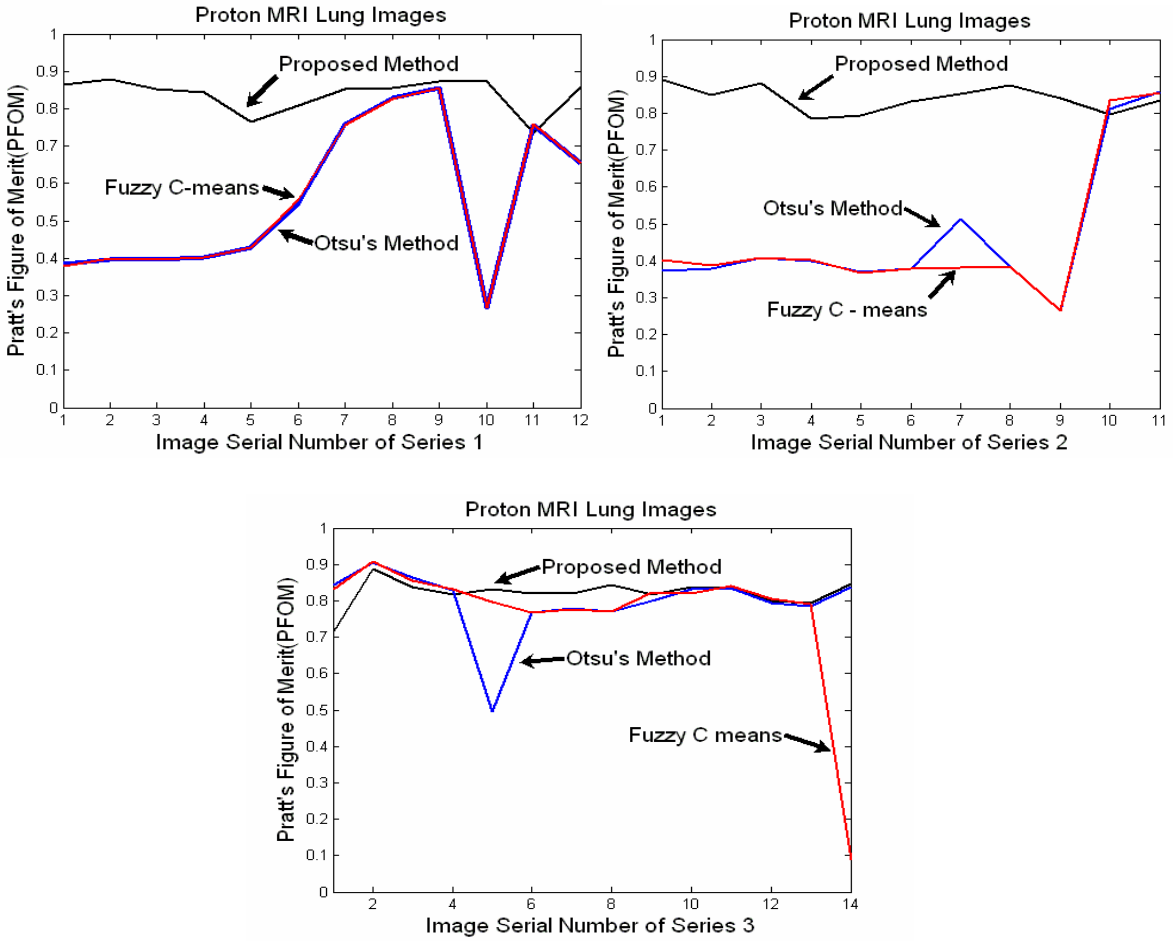

Fig. 4: PFOM for our proposed method on three sets of lung MRI slices from three study series.

We have computed PFOM to measure the quantitative evaluation of the lung boundary extraction results. PFOM is a dimensionless number between 0 and 1, with 1 for ideal segmentation. To compute PFOM we need the ideal edges that are computed by manually segmented lung boundaries. We perform automated segmentation on three MRI data sets. The segmentation process as explained already consists of VM thresholding followed by morphological post processing. To compare our segmentation results with other methods, we replace the thresholding step by other binarization algorithms. The PFOM results of all MRI slices over the three data sets are shown in Fig. 4. Table 1 summarizes the average value of PFOM of all three data sets and it compares the results found by Ray *et al.*'s active contour method [15], Otsu's method and fuzzy *c*-means. Results found by our proposed method shows superiority over the other results.

MRI data sets (Series Number)	PFOM value (proposed method)	PFOM value (Ray *et al.*'s method [15])	PFOM value (Otsu's Method)	PFOM value (Fuzzy *c*-means)
1	0.8381	0.7156	0.5565	0.5567
2	0.8395	0.7120	0.4672	0.4607
3	0.7955	0.7085	0.7954	0.7648

Table 1: Comparison of our segmentation method with Ray *et al.*, Otsu and Fuzzy *c*-means methods using Pratt's figure of merit (PFOM).

4.2 Preserving Texture information

To examine the performance of the proposed algorithm on preservation of texture and edges, we apply it on 512 x 512 grayscale Barbara image (shown in Fig. 5(a)). The result is shown in Fig. 5(b). Here, the value of q is taken as 1.5. We have implemented Liu *et al.*'s method on the Barbara image and we have chosen the two tuning parameters of their method $\sigma = 16$, $w = 1$ from their article [11]. We have also implemented Otsu's global thresholding and fuzzy *c*-means on the same image as shown in Fig.5. These results show that our proposed method can preserve better texture/edge information.

We further experiment with our proposed method on some benchmark images: Girl (Fig. 6), Truck (Fig. 7), and Tank (Fig. 8) used in image processing literature. Once again, from Fig. 6 it is observed that our proposed method can preserve better texture information on Girl image (especially top left quadrant of the image shown in Fig. 6(b)) than other competitive methods. Our method also works well on both the well known truck and tank images. It can segment the wheel of the truck (shown in Fig. 7(b)) and the star sign located on the tank (shown in Fig. 8(b)) from their noisy backgrounds, whereas the other methods fail to retain such texture information.

(a) Barbara image

(a) Proposed method

(b) Liu *et al*.'s method [11]

(c) Otsu's method [14]

(d) Fuzzy *c*-means.

Fig. 5: Thresholded Barbara image.

(a) GIRL image

(b) Proposed method

(c) Liu *et al*.'s method [11]

(d) Otsu's method [14]

(e) Fuzzy *C*- means

Fig 6: GIRL image and results of different segmentation techniques.

(a) Truck image

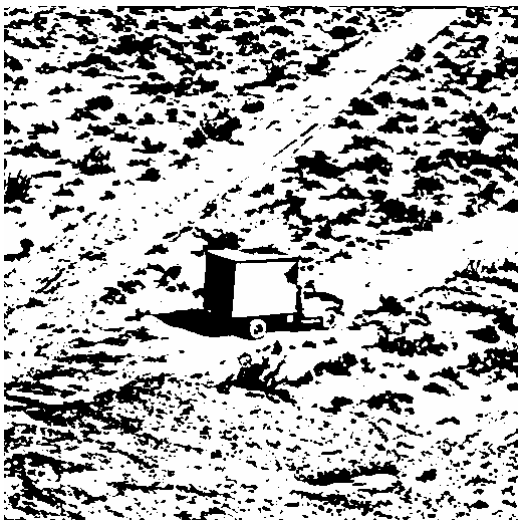

(b) Proposed method

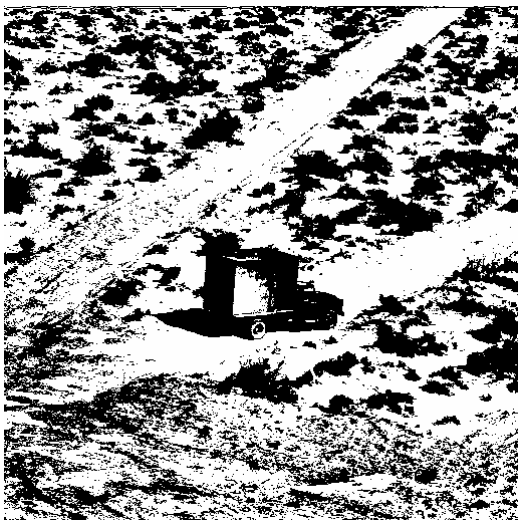

(c) Liu *et al.*'s method [11]

(d) Otsu's method [14]

(e) Fuzzy *C*- means

Fig 7: Truck image and results of different segmentation techniques

(a) Tank image

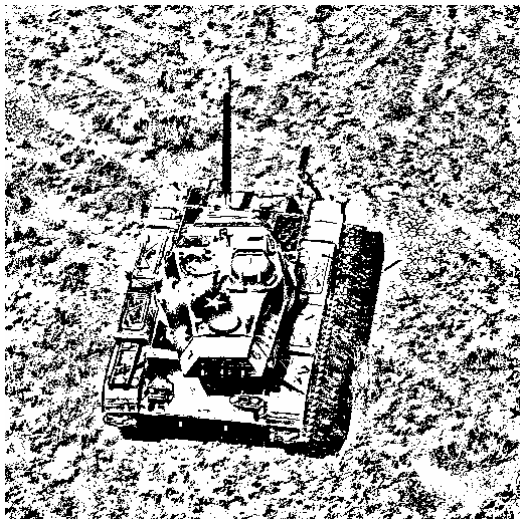

(b) Proposed Method

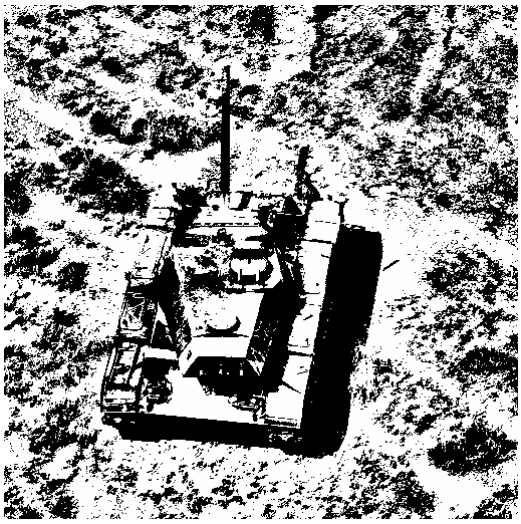

(c) Liu *et al*.'s method [11]

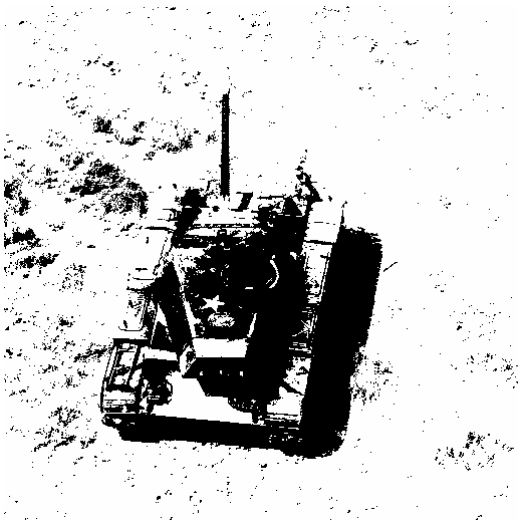

(d) Otsu's method [14]

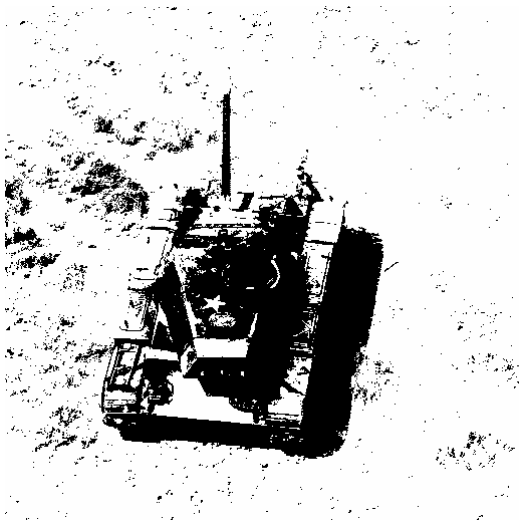

(e) Fuzzy c – means

Fig. 8: Tank image and results of different segmentation techniques.

4.3 Comparison of VM with Fibonacci Search

Here, we show experimentally that the proposed method is computationally more attractive than a conventional Fibonacci search applied to find the minimax solution of the proposed energy functional. In Fibonacci search the value of the weighting parameter α is chosen according to a Fibonacci sequence. Next, the energy functional is minimized with respect to the threshold function T for each value of α. As $\alpha \in [0, 1]$, we have chosen the value of α initially as 0.1, 0.2 and 0.3 respectively. For each value of α, $\min_T E(T;\alpha)$ is computed. As the energy functional is convex with respect to α, we need to compute $\min_T E(T;\alpha)$ for three consecutive values of α in a Fibonacci sequence to reach at the maximum point on the energy curve shown in Fig. 9. There are three cases which might occur:

1. If $\min_T E(T;\alpha)$ at any three consecutive values of α in a Fibonacci sequence are monotonically increasing in order, then the maximum point occurs beyond the largest of the three α values.

2. If $\min_T E(T;\alpha)$ for three values of α say α_1, α_2 and α_3 are respectively T_1, T_2 and T_3, where $T_1 < T_2 > T_3$ and $\alpha_1 < \alpha_2 < \alpha_3$, then the maximum point at the curve lies between α_1 and α_3.

3. If $\min_T E(T;\alpha)$ at any three consecutive values of α in a Fibonacci sequence are monotonically decreasing in order, then the maximum point occurs before the smallest of the three α values.

In case 1 and 3 further search is performed until case 2 is found. In case 2, further search is conducted with a decreased order of α values (if the values of α were 0.1, 0.2, 0.3 they will now be 0.01, 0.02, 0.03 etc.) and the search is finally stopped when a desired

accuracy for α is reached. A typical behaviour of the energy functional with respect to α is shown in Fig. 9.

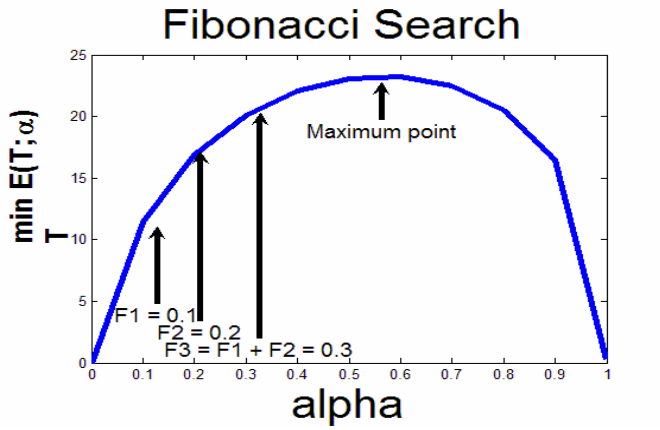

Fig. 9. Behaviour of the energy functional with respect to α.

Note that the performance of Fibonacci search-based minimax solution depends on two criteria: (a) the order of the value of weighting parameter α at which search is stopped (b) the maximum number of iterations required to converge $\min_T E(T;\alpha)$ for each value of α using gradient descent technique with line search.

We have carried out experiment on Barbara image shown in Fig. 5(a). Our proposed method converges after *129* iterations. The performance of Fibonacci search-based minimax solution is shown in Table 2. To keep the comparison fair, we stop the VM at the same accuracy level of α as the Fibbonacci search.

Maximum # of iterations to find $\min_T E(T;\alpha)$	Total # of iterations to find minimax solution
100	809
200	1109
500	2009
1000	3509

Table 2: Performance of Fibonacci search-based minimax solution.

5. Conclusion and Future Work

In this paper we introduce a variational adaptive image thresholding technique where we design a novel energy functional consisting of a data term and a regularization term, encouraging the threshold surface, respectively to intersect the image surface only at high gradient places, and to enforce smoothness in the threshold surface. There is a weighting parameter that makes a balance between the data term and the regularization term and it tries to contravene the domination of one term over other. The optimal value of the weighting parameter as well as the desired threshold surface is computed through an iterative minimax algorithm. Our algorithm attempts to mitigate the user effort to adjust the values of the weighting parameter. Moreover, it avoids multiple minima computation as in Fibonacci search-based minimax solution method to substantially save on computations. The method shows encouraging results when utilized to find lung boundaries on proton MR images. The method is also shown to preserve texture and edge better than other competing methods.

A few future plans about the proposed VM method are as follows. We would like to concentrate an automated technique where simultaneous smoothing and thresholding operations of the images can be performed in a cooperative manner so that it can mostly eliminate the work of post processing. Here, we propose to determine the value of the edge indicator index, q experimentally for the lung boundary extraction applications. Although a very small number of training images is usually good enough for this estimation, in the future, we would like to concentrate on finding the value of q automatically from the data. Further, here we have chosen a particular convex combination of data and regularization term. Our future endeavor will investigate whether other convex combination of data and regularization terms works successfully in different applications. At present, our method is purely an edge based thresholding

technique. We also would want to incorporate the gray level histogram information in the VM algorithm and get the advantage of both edge and region based segmentation techniques.

Acknowledgement: This work is supported by NSERC, iCORE, and University of Alberta.

Appendix

A. *E* is a concave function with respect to α.

To prove E is concave in α, it is required to show that for any $\alpha \in [0, 1]$: $\frac{\delta^2 E(\alpha,T)}{\delta\alpha^2} < 0$.

Note that: $\frac{\delta E(\alpha,T)}{\delta\alpha} = E_2(T) - \frac{\alpha E_1(T)}{\sqrt{1-\alpha^2}}$, and $\frac{\delta^2 E(\alpha,T)}{\delta\alpha^2} = -\frac{E_1(T)}{(1-\alpha^2)^{\frac{3}{2}}} < 0$. So E is concave in α.

B. *E* (*T*; α) is strictly convex in *T*.

In order to prove *E* (*T*; α) is strictly convex in *T*, we need to show $E(T+U;\alpha) - E(T;\alpha) \geq \delta E(T;\alpha)$ holds for $\forall U$ such that $T+U \in D$ [20]. By substituting the variational minimax functional, we have

$$E(T+U;\alpha) - E(T;\alpha) = \sqrt{1-\alpha^2}\iint h(I-T-U)^2 + \alpha\iint|\nabla(T+U)|^2 - \sqrt{1-\alpha^2}\iint h(I-T)^2 - \alpha\iint|\nabla T|^2$$

$$= \sqrt{1-\alpha^2}\iint\left(h\left((I-T)^2 + U^2 - 2(I-T)U\right)\right) + \alpha\iint\left(|\nabla T|^2 + |\nabla U|^2 + 2\nabla T.\nabla U\right)$$
$$- \sqrt{1-\alpha^2}\iint h(I-T)^2 - \alpha\iint|\nabla T|^2$$

$$= \sqrt{1-\alpha^2}\iint\left(h\left(U^2 - 2(I-T)U\right)\right) + \alpha\iint\left(|\nabla U|^2 + 2\nabla T.\nabla U\right).$$

Similarly, we can show

$$E(T+\varepsilon U;\alpha) - E(T;\alpha) = \sqrt{1-\alpha^2}\iint\left(h(x,y)\left(\varepsilon^2U^2 - 2\varepsilon(I-T)U\right)\right) + \alpha\iint\left(\varepsilon^2|\nabla U|^2 + 2\varepsilon\nabla T.\nabla U\right)$$

Therefore, the Gâteaux variation of variational minimax functional is given by

$$\delta E(T;\alpha) = \lim_{\varepsilon \to 0} \frac{E(T+\varepsilon U;\alpha) - E(T;\alpha)}{\varepsilon}$$

$$= \lim_{\varepsilon \to 0} (\sqrt{1-\alpha^2} \iint h(\varepsilon U^2 - 2(I-T)U) + \alpha \iint \varepsilon |\nabla U|^2 + 2\nabla T.\nabla U)$$

$$= \sqrt{1-\alpha^2} \iint (h(-2(I-T)U)) + \alpha \iint 2\nabla T.\nabla U.$$

Thus, we have

$$E(T+U;\alpha) - E(T;\alpha) - \delta E(T;\alpha) = \sqrt{1-\alpha^2} \iint h(x,y)U^2 + \alpha \iint |\nabla U|^2$$

Since, both α *and* $\sqrt{1-\alpha^2}$ and $h(x, y)$ are non negative $\forall \alpha \in [0,1]$, we have

$$E(T+U;\alpha) - E(T;\alpha) - \delta E(T;\alpha) \geq 0$$

The equality holds if and only if $U = 0$. Hence, $E(T; \alpha)$ is strictly convex in T.

C. Minimization of the energy functional using calculus of variation

For a fixed value of α, say α^*, proposed energy functional E becomes,

$$E = \frac{1}{2}\sqrt{1-(\alpha^*)^2} \iint h(x,y)(I(x,y) - T(x,y))^2 \, dxdy + \frac{1}{2}\alpha^* \iint |\nabla T(x,y)|^2 \, dxdy$$

Now, Euler equation, $E_f = E_T - E_{T_x} - E_{T_y}$, where $E_T = \frac{\partial E}{\partial T}$, $T_x = \frac{\partial T}{\partial x}$, $T_y = \frac{\partial T}{\partial y}$

$$E_T = -\sqrt{1-(\alpha^*)^2}\, h(x,y)(I(x,y) - T(x,y))$$

$$E_{T_x} = \frac{\partial E}{\partial T_x} = \alpha^* T_{xx}, T_{xx} = \frac{\partial^2 T}{\partial x^2}$$

$$E_{T_y} = \frac{\partial E}{\partial T_y} = \alpha^* T_{yy}, T_{yy} = \frac{\partial^2 T}{\partial y^2},$$

Using Gradient Descent Technique [20] we have,

$$\frac{\partial T(x,y)}{\partial t} = -E_f$$

$$= \sqrt{1-(\alpha^*)^2}\, h(x,y)(I(x,y) - T(x,y)) + \alpha^*(T_{xx} + T_{yy}),$$

$$= \sqrt{1-(\alpha^*)^2}\, h(x,y)(I(x,y) - T(x,y)) + \alpha^*(\nabla^2 T).$$

D. Line search details

Let $E(T^{(k)}+\tau^{(k)}\delta T^{(k)}) = E_1 + E_2$, where,

$$E_1 = \frac{\alpha^{(k)}}{2}\sum\left\|\nabla\left(T+\tau^{(k)}\delta T\right)\right\|^2$$
$$= \frac{\alpha^{(k)}}{2}\sum\left\|\nabla T+\tau^{(k)}\nabla\left(\delta T\right)\right\|^2$$
$$= \frac{\alpha^{(k)}}{2}\sum\left\|\nabla T\right\|^2+\alpha^{(k)}\tau^{(k)}\sum\left(\nabla T.\nabla\left(\delta T\right)\right)+\frac{\alpha^{(k)}(\tau^{(k)})^2}{2}\sum\left\|\nabla\delta T\right\|^2,$$

and

$$E_2 = \frac{\sqrt{1-\left(\alpha^{(k)}\right)^2}\,h(x,y)}{2}\sum\left(I-T-\tau^{(k)}\delta T\right)^2$$
$$= \sqrt{1-\left(\alpha^{(k)}\right)^2}\,h(x,y)\left\{\frac{1}{2}\sum\left(I-T\right)^2-\tau^{(k)}\sum\left(I-T\right)\left(\delta T\right)+\frac{(\tau^{(k)})^2}{2}\sum\left(\delta T\right)^2\right\}.$$

So,

$$E_1+E_2 = \frac{1}{2}\sum\left\{\alpha^{(k)}\left\|\nabla T\right\|^2+\sqrt{1-\left(\alpha^{(k)}\right)^2}\,h(x,y)\left(I-T\right)^2\right\}+$$
$$\tau^{(k)}\left[\sum\left\{\alpha^{(k)}\left(\nabla T.\nabla\left(\delta T\right)\right)-\sqrt{1-\left(\alpha^{(k)}\right)^2}\,h(x,y)\left(I-T\right)\left(\delta T\right)\right\}\right]$$
$$+\frac{(\tau^{(k)})^2}{2}\sum\left\{\sqrt{1-\left(\alpha^{(k)}\right)^2}\,h(x,y)\left(\delta T\right)^2+\alpha^{(k)}\left\|\nabla\delta T\right\|^2\right\}$$
$$= e_1+\tau^{(k)}e_2+(\tau^{(k)})^2e_3,$$

where, $e_1 = \frac{1}{2}\sum\left\{\alpha^{(k)}\left\|\nabla T\right\|^2+\sqrt{1-\left(\alpha^{(k)}\right)^2}\,h\left(I-T\right)^2\right\},$

$$e_2 = \sum\left\{\alpha^{(k)}\left(\nabla T.\nabla\left(\delta T\right)\right)-\sqrt{1-\left(\alpha^{(k)}\right)^2}\,h\left(I-T\right)\left(\delta T\right)\right\},$$

and $e_3 = \frac{1}{2}\sum\left\{\sqrt{1-\left(\alpha^{(k)}\right)^2}\,h\left(\delta T\right)^2+\alpha^{(k)}\left\|\nabla\delta T\right\|^2\right\}.$

References

[1] I. E. Abdou and W. K. Pratt, "Quantitative design and evaluation of enhancement/ thresholding edge detectors," *proceedings of the IEEE*, vol. 67, No. 5, pp. 753-763, may 1979.

[2] F. H. Y. Chan, F.K. Lam and Hui Zhu, "Adaptive Thresholding by Variational Method," *IEEE Transactions on Image Processing*, vol. 7, No. 3, pp. 468- 473, march 1998.

[3] C. K. Chow and T. Kaneko, "Automatic boundary detection of the left-ventricle from cineangiograms," *Computers and Biomedical Research*, Vol. 5, pp. 388-410, 1972.

[4] G. Evans, J. Blackledge and P. Yardley, *Numerical Methods for Partial Differential Equations*, Springer, 2005.

[5] R. Fletcher, “Practical Methods of Optimization,” Second Edition, *John Wiley & Sons*, 2006.

[6] M. A. Gennert and A. Y. Yuille, “Determining the optimal weights in multiple objective function optimization,” *Proc. Second Int. Conf. Computer Vision*, pp. 87-89, 1988.

[7] R. C. Gonzalez and R. E. Woods, *Digital Image Processing*, Pearson prentice Hall, 2005.

[8] J. Kittler and J. Illingworth, “ Minimum error thresholding,” *pattern Recognition*, Vol. 19, No. 1, pp. 41-47, 1986.

[9] R. Jain, R. Kasturi, and B. G. Schunk, *Machine Vision*. New York: McGraw – Hill, 1995.

[10] Xiang Li, Rahul Ramachandran, Matt he, Sunil Movva, John Rushing, Sara Graves, Wladislaw Lyatsky, Arjun Tan and Glynn Germany , “ Comparing Different Thresholding Algorithms for Segmenting Auroras,” *Proceedings of the International Conference on Information Technology: Coding and Computing*, Vol. 2, pp. 594 – 601,2004.

[11] F. Liu, Y. Luo, X. Song and D. Hu, “Active surface model-based adaptive thresholding algorithm by repulsive external force,” *J. of Electronic Imaging*, vol.12, pp.299-306, 2003.

[12] D. L. Milgram, A. Rosenfeld, T. Willet, and G. Tisdale, “Algorithms and hardware technology for image recognition,” *Final Report to U.S. Army Night Vision Laboratory*, Comput. Sci. Ctr., Univ. Maryland, College park, 1978.

[13] W. Niblack, *An Introduction to Digital Image Processing*, Prentice-Hall, Englewood Cliffs, NJ, 1986.

[14] N. Otsu, “A threshold selection method from gray– level histogram,” *IEEE Transactions on System Man Cybernatics*, Vol. SMC-9, No.1, pp. 62-66, 1979.

[15] N. Ray, S. T. Acton, T. Altes, E. E. de Lange and J. R. Brookeman, “Merging parametric active contours within Homogeneous Image Regions for MRI-Based Lung Segmentation,” *IEEE Trans. Med. Imaging,* Vol. 22, pp. 189-199, Feb. 2003.

[16] Andrzej Ruszczynski, “ Nonlinear Optimization, *Princeton university Press*, 2006

[17] P.K. Sahoo, S. Soltani, A.K.C. Wong, and Y. Chen, “A survey of thresholding techniques,” *Computer Vision Graphics Image Processing*, Vol. 41, 1988, pp. 233 – 260.

[18] M. Sezgin and B. Sankur, “Survey over image thresholding techniques and quantitative performance evaluation,” *Journal of Electronic Imaging*, vol. 13, pp. 146-165, 2004.

[19] D. Shen and H. H. S. Ip, “A Hopfield neural network for adaptive image segmentation: An active surface paradigm,” *Pattern Recogn. Lett*. Vol . 18, pp. 37 - 48 , 1997.

[20] John L. Troutman, “ Variational Calculus with Elementary Convexity,” *Springer – Verlag*, 1983.

[21] F. Yan, H. Zhang, and C. R. Kube, “Multistage Adaptive Thresholding Method,” *Pattern Recognition Letters*, Volume 26, Issue 8, pp. 1183-1191, June, 2005.

[22] S. D. Yanowitz and A. M. Bruckstein, “A new method for image segmentation,” *Comput. Vision, Graphs, image process*, vol. 46, pp. 82-95, 1989.